# Effects of Nonuniform Beam Filling on Rainfall Retrieval for the TRMM Precipitation Radar

S. L. DURDEN, Z. S. HADDAD, A. KITIYAKARA, AND F. K. LI

*Jet Propulsion Laboratory, California Institute of Technology, Pasadena, California*

(Manuscript received 18 April 1997, in final form 21 August 1997)

ABSTRACT

The Tropical Rainfall Measuring Mission (TRMM) will carry the first spaceborne radar for rainfall observation. Because the TRMM Precipitation Radar (PR) footprint size of 4.3 km is greater than the scale of some convective rainfall events, there is concern that nonuniform filling of the PR antenna beam may bias the retrieved rain-rate profile. The authors investigate this effect theoretically and then observationally using data from the NASA Jet Propulsion Laboratory Airborne Rain Mapping Radar (ARMAR), acquired during Tropical Oceans Global Atmosphere Coupled Ocean–Atmosphere Response Experiment in early 1993. The authors' observational approach is to simulate TRMM PR data using the ARMAR data and compare the radar observables and retrieved rain rate from the simulated PR data with those corresponding to the high-resolution radar measurements. The authors find that the path-integrated attenuation and the resulting path-averaged rain rate are underestimated. The reflectivity and rain rate near the top of the rainfall column are overestimated. The near-surface reflectivity can be overestimated or underestimated, with a mean error very close to zero. The near-surface rain rate, however, is usually underestimated, sometimes severely.

## 1. Introduction

The Tropical Rainfall Measuring Mission (TRMM) will carry the first spaceborne radar for rainfall observation (Simpson et al. 1988). While the TRMM Precipitation Radar (PR) footprint size of 4.3 km is small when compared with typical spaceborne passive microwave sensors, it is larger than the typical size of rain cells. Goldhirsh and Musiani (1986), for example, found that the median convective cell size for convective storms off the Virginia coast is only 1.9 km. This implies that the rainfall within the PR footprint may not be uniformly spread when observing convective rainfall. Analyses of such nonuniform beam filling (NUBF) for passive microwave sensors have found biases in the estimated rainfall (Graves 1993; Ha and North 1995), and the passive retrieval algorithm of Kummerow and Giglio (1994) includes a technique to correct for NUBF effects. Biases in radar-retrieved rain rate due to NUBF have been found by a number of authors using simulated data or data from ground-based radar (Nakamura 1991; Amayenc et al. 1993; Testud et al. 1996). Amayenc et al. (1996) found bias due to NUBF using data from a nadir-looking aircraft radar for a rainstorm off the U.S. Atlantic coast. Kozu and Iguchi (1996) proposed an algorithm for correcting biases due to NUBF and evaluated the algorithm using ship-based radar data.

In this work, we investigate the statistical nature of NUBF effects on TRMM PR measurements using a large dataset acquired by the National Aeronautics and Space Administration/Jet Propulsion Laboratory (NASA/JPL) Airborne Rain Mapping Radar (ARMAR) during the Tropical Oceans Global Atmosphere Coupled Ocean–Atmosphere Response Experiment (TOGA COARE) (Webster and Lukas 1992). Data from ARMAR is well suited for such a study because it operates with the same frequency and downward-looking geometry as the TRMM PR but has substantially better spatial resolution (0.8 km at the surface). The ARMAR TOGA COARE dataset is ideal for TRMM PR studies because it consists of extensive measurements of oceanic mesoscale convective systems, which are expected to be typical of the type of rainfall that TRMM will observe. The methodology for this study consists of simulating the TRMM PR using the ARMAR TOGA COARE data, retrieving rainfall rate from the simulated PR data, and comparing the result with rain rates retrieved from the higher horizontal resolution ARMAR data. This study differs from previous work in its use of data at the TRMM PR frequency and in the large volume of data used, allowing NUBF bias statistics to be derived. In addition to rain-rate biases, we also examine biases in the radar reflectivity and path-integrated attenuation. We begin by presenting a brief discussion of the ARMAR TOGA COARE dataset. This is fol-

*Corresponding author address:* Dr. Stephen L. Durden, JPL—Mail Stop 300-227, 4800 Oak Grove Drive, Pasadena, CA 91109.
E-mail: durden@kappa.jpl.nasa.gov

TABLE 1. Comparison of ARMAR and TRMM PR parameters.

| Parameter | ARMAR | TRMM |
|---|---|---|
| Frequency | 13.8 GHz | 13.8 GHz |
| Scanning swath | 9 km | 220 km |
| Scan angles | $\pm 20^\circ$ | $\pm 17^\circ$ |
| Surface horizontal resolution | 800 m | 4.3 km |
| Range resolution | 80 m | 250 m |
| Noise floor (at surface) | 10 dBZ | 23 dBZ |
| Samples | >100 | 64 |

lowed by a review of rain retrieval theory and a theoretical discussion of the NUBF problem. The simulation technique and errors due to NUBF, as derived from the ARMAR data, are then presented.

## 2. TOGA COARE data characteristics

TOGA COARE was an international field experiment carried out in the western Pacific Ocean in 1992–93. The NASA DC-8 aircraft flew a total of 13 TOGA COARE missions in January and February 1993. It was equipped with the ARMAR radar system, as well as a variety of other instruments for remote sensing and in situ measurements. ARMAR is a multipolarization Doppler radar designed to support TRMM PR retrieval algorithm development and TRMM postlaunch validation activities. ARMAR operates at the PR frequency of 13.8 GHz (Ku band) and uses a scanning geometry similar to the PR, scanning its antenna across track $\pm 20^\circ$. Calibration of the reflectivity was accomplished using a calibration loop, which couples a portion of the transmitted power to the receiver (Durden et al. 1994). Calibration was verified by comparing the measured clear-air ocean backscatter cross section $\sigma^\circ$ at 10° incidence with measurements reported by Schroeder et al. (1985). The measurements agree to within about $\pm 1$ dB. ARMAR characteristics are shown in Table 1, along with the corresponding characteristics of the PR. Additional details on ARMAR hardware and data processing can be found in Durden et al. (1994).

During TOGA COARE, most of the precipitation observed by ARMAR was associated with mesoscale convective systems. As discussed by Houze (1981), precipitation can be classified as either stratiform or convective. Stratiform rain is associated with areas of weak vertical motion and is produced as ice particles sink and melt. Stratiform rain is usually much lighter, more spatially uniform, and more spatially extensive than convective rain. In radar imagery it can typically be recognized by the presence of a region of high reflectivity, called the bright band, located just below the 0°C isotherm. Convective rainfall, on the other hand, is produced in regions of intense updrafts and downdrafts. It can have much higher rain rates and larger horizontal variability than stratiform rain. The ARMAR data used in this work consist of numerous flight lines over mesoscale convective systems and include observations of both convective and stratiform rain.

## 3. Theory of NUBF effects

Estimation of rain rate from radar observations has been pursued for many years. At lower frequencies (e.g., 3 GHz) attenuation due to rainfall is generally small and the rainfall rate has typically been retrieved from radar observations using $Z$–$R$ relations, which relate the radar reflectivity factor $Z$ to the rainfall rate $R$ by a power law, $Z = aR^b$. However, at the higher frequencies typically used for airborne and spaceborne radars, attenuation is larger and cannot, in general, be neglected. In this case the measured reflectivity $Z^m$ is related to the reflectivity $Z$ by

$$Z^m(r) = Z(r)10^{-0.2\int_0^r k(s)ds}, \tag{1}$$

where $r$ is range and $k$ is the specific attenuation. Recovery of both the $Z$ and $k$ profiles given only $Z^m$ is underdetermined. However, by assuming a $k$–$R$ relation of the form $k = \alpha R^\beta$, as well as a $Z$–$R$ relation, (1) can be rewritten as

$$Z^m(r) = aR(r)^b 10^{-0.2\int_0^r \alpha R(s)^\beta ds}. \tag{2}$$

Equation (2) can be solved analytically for $R(r)$ given $Z^m(r)$ (Hitschfeld and Bordan 1954). As discussed by Hitschfeld and Bordan (1954) and Meneghini (1978), direct numerical evaluation of the analytical solution of (2) can become unstable at higher rain rates unless an auxiliary measurement of rain rate or attenuation is used. For a downward-looking airborne or spaceborne radar, an independent measurement of the path-integrated attenuation (PIA) can be used, and a technique for obtaining such a measurement is the surface reference technique (SRT), first proposed by Meneghini et al. (1983). In the SRT a radar measurement of the ocean surface in a clear area is compared with the measurement in the raining area; the difference is assumed to be due only to the rainfall attenuation and provides an estimate of the two-way PIA. Several algorithms that combine the Hitschfeld–Bordan (HB) solution with the SRT-measured PIA have been presented in the literature (e.g., Meneghini et al. 1983; Marzoug and Amayenc 1994). While details vary, they are similar in principle. Iguchi and Meneghini (1994) show the relations between the various algorithms and also propose a hybrid technique that combines the HB solution with the SRT in moderate and heavy rain but uses only the HB solution in light rain.

Implicit in the above discussion is the uniformity of the rain rate across the antenna beam. When this is not the case, the retrieval of the rain rate $\langle R \rangle$ averaged across the beam is desired (e.g., Amayenc et al. 1996). For a nadir-looking radar, this averaging would occur in the horizontal plane. If the horizontally averaged rain $\langle R \rangle$ were spread uniformly across the beam, the radar would measure

$$Z_u^m(r) = a\langle R(r)\rangle^b 10^{-0.2\int_0^r \alpha\langle R(s)\rangle^\beta ds}, \quad (3)$$

where the subscript $u$ denotes ''uniform.'' Equation (3) is simply (2) with $R(r)$ replaced by $\langle R(r)\rangle$. It is thus obvious that $\langle R\rangle$ can be retrieved by the same methods as applied to (2). Unfortunately, the radar does not measure (3). Instead, it takes the horizontal average of (2), giving

$$Z_a^m(r) = \langle aR(r)^b 10^{-0.2\int_0^r \alpha R(s)^\beta ds}\rangle, \quad (4)$$

where the subscript $a$ denotes ''apparent.'' When the $Z$–$R$ relation is linear ($b = 1$) and attenuation is negligible, (3) and (4) are equivalent. However, in general, nonlinearity is present in both the $Z$–$R$ relation and the relation of the rain rate to the attenuation (as expressed in the linear domain). The latter is highly nonlinear, even when the $k$–$R$ relation itself is linear (i.e., $\beta = 1$). In this general case, (3) and (4) differ, and it is impossible to express the radar measurement (4) in terms of $\langle R\rangle$. The difference between apparent and uniform quantities is the error due to NUBF and is the focus of this paper, although the reader should realize that there is a variety of error sources in rain retrieval in addition to NUBF effects.

NUBF effects can be investigated theoretically by viewing the rain rates in a given range bin as being samples of a single random variable. In this case the averages across the antenna beam, denoted by $\langle\cdot\rangle$, can be computed as statistical expectations. Using the SRT, a spaceborne radar would measure the following PIA:

$$A_a = \langle 10^{-0.2\int_0^L \alpha R(s)^\beta ds}\rangle, \quad (5)$$

where, as before, the subscript $a$ denotes apparent and $L$ is the rain layer depth. It is convenient to relate the PIA to $R_p$, the path-averaged rain rate (PARR), defined as $R_p = L^{-1}\int_0^L R(s)\,ds$. For an arbitrary value of $\beta$ the integral in (5) cannot be expressed in terms of $R_p$. In practice, however, $\beta$ is very close to unity (Olsen et al. 1978), so (5) can be well approximated by the following (Meneghini et al. 1983):

$$A_a = \langle 10^{-0.2L\alpha R^\beta}\rangle. \quad (6)$$

This approximation simplifies our analysis and should not substantially affect our results. The PIA corresponding to the horizontally averaged PARR, after being distributed uniformly over the antenna beam, is

$$A_u = 10^{-0.2L\alpha\langle R_p\rangle^\beta}, \quad (7)$$

where the subscript $u$ denotes uniform.

Near the top of the rain column, where attenuation can be neglected, the apparent reflectivity is

$$Z_a^m = a\langle R^b\rangle, \quad (8)$$

while the uniform reflectivity, corresponding to the horizontally averaged rain rate, is

$$Z_u^m = a\langle R\rangle^b. \quad (9)$$

The reflectivity measured by a spaceborne system near the surface, where attenuation is maximum, is

$$Z_a^m = a\langle R^b 10^{-0.2L\alpha R_p^\beta}\rangle, \quad (10)$$

where $R$ is the rain rate in a thin layer near the surface and $R_p$ is the path-averaged rain rate in the path above the thin layer. The near-surface reflectivity corresponding to the horizontally averaged near-surface rain rate $\langle R\rangle$ and the horizontally averaged PARR $\langle R_p\rangle$ is

$$Z_u^m = a\langle R\rangle^b 10^{-0.2L\alpha\langle R_p\rangle^\beta}. \quad (11)$$

To perform computations using (6)–(11), we assume that the rain depth $L$ is 4.5 km and we use the following relations (Nakamura et al. 1990):

$$k = 0.032R^{1.124} \quad (12)$$

and

$$Z = 372.4R^{1.54}. \quad (13)$$

In addition, we assume that the rain rate sampled over the antenna footprint is a lognormal random variable (Lopez 1977; Kedem et al. 1990; Kozu and Iguchi 1996):

$$p(R) = \frac{1}{\sqrt{2\pi}\,\xi R}\exp\left(-\frac{(\ln R - \mu)^2}{2\xi^2}\right), \quad (14)$$

where $\mu$ and $\xi^2$ are the mean and variance, respectively, of $\ln R$. The mean of $R$ is $\exp(\mu + \xi^2/2)$, and its normalized standard deviation $\sigma$ is $(\exp\xi^2 - 1)^{1/2}$. At the top of the rain column, where attenuation is negligible, the ratio of the apparent reflectivity to the uniform reflectivity, corresponding to the horizontally averaged rain rate, can be found analytically:

$$\frac{Z_a^m}{Z_u^m} = \frac{\langle R^b\rangle}{\langle R\rangle^b} = (\sigma^2 + 1)^{b(b-1)/2}. \quad (15)$$

In this case the error is independent of the rain-rate mean and depends only on the normalized rain-rate standard deviation $\sigma$. For the case of $\sigma = 1$, that is, the rain-rate standard deviation equal to the rain-rate mean, we find that the reflectivity is overestimated by 1.25 dB (i.e., $Z_a^m > Z_u^m$). For $\sigma = 0.2$ the overestimation is reduced to less than 0.1 dB. The overestimation is due to the nonlinearity of the $Z$–$R$ relation; it is 0 dB for $b = 1$ and increases as $b$ is increased. The rain rate derived from the apparent reflectivity is also overestimated. These results are in agreement with the simple model of an area that is half-clear and half-filled with uniform rain, analyzed by Nakamura (1991). Nakamura's simple model is mathematically equivalent to our formulation in which the rain rate is a random variable but with a binary rather than lognormal distribution. In the binary case the rain rate takes only the values zero or $R$, each with a probability of one-half. This model is much simpler to conceptualize than the lognormal model and may be crudely representative of the situation in which the antenna beam includes the edge of a raining area.

The errors due to NUBF for PIA and near-surface reflectivity are calculated numerically for the lognormal

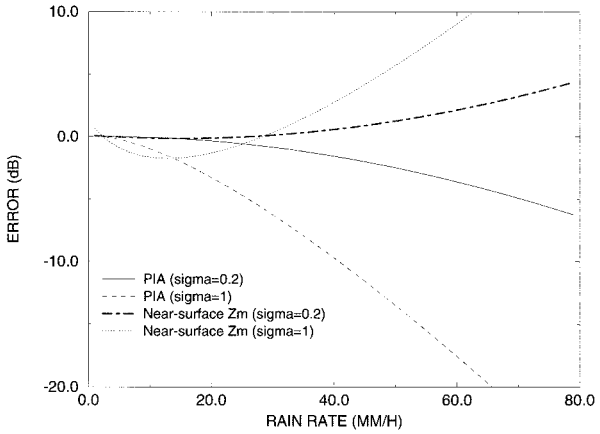


FIG. 1. Calculated NUBF errors in two-way PIA and near-surface reflectivity (apparent minus uniform) for a lognormal rain rate, as a function of the mean rain rate, for normalized rain-rate standard deviations $\sigma = 0.2$ and $\sigma = 1$.

rain-rate distribution. For simplicity, it is assumed that the rain rate is perfectly correlated in the vertical direction. The ARMAR data, in contrast, indicate that substantial decorrelation in the vertical may occur; this reduces the magnitude of the NUBF errors since the effects due to each level do not compound coherently. Thus, the results here can be considered worst case. We compare the two-way PIAs as expressed in decibels; that is, we compute the negative of 10 log $A$, so that PIAs are positive numbers. A larger PIA expressed in decibels corresponds to a smaller $A$ in the linear domain. Figure 1 shows the PIA error versus rain rate for a lognormal rain rate with $\sigma = 0.2$ and $\sigma = 1$; the error is defined as the apparent PIA in decibels minus the uniform PIA. The error is always negative ($A_a > A_u$ in the linear domain) and becomes large at high rain rates. The error for different choices of $\sigma$ has essentially identical qualitative behavior versus rain rate; however, the error magnitude increases for increasing $\sigma$. The PIA underestimation in Fig. 1 is due to the exponential dependence of the attenuation on rain rate and was also noted for the half-filled (or binary) model of Nakamura (1991). The average rain rate is one-half the rain rate of the raining area and can thus correspond to a large uniform attenuation. The apparent attenuation in the binary model, however, is less than 3 dB and is always underestimated. The PARR derived from the apparent PIA in both the lognormal and binary models would also be underestimated.

Figure 1 also shows the error in the measured near-surface reflectivity versus rain rate for the lognormal rain model with $\sigma = 0.2$ and $\sigma = 1$. The near-surface reflectivity is slightly overestimated at very low rain rates (approximately 1 mm h$^{-1}$), underestimated at moderate rain rates, and severely overestimated at high rain rates. The overestimation at very low rain rates is due to the nonlinearity of the $Z$–$R$ relation. The behavior at moderate to high rain rates is due primarily to the exponential dependence of the attenuation on rain rate; the $Z$–$R$ relation nonlinearity does not have a major impact. In fact, repeating the calculations with $b = 1$ yielded similar results, except that overestimation does not occur at very low rain rates. As was true for the PIA error, the near-surface reflectivity error for different choices of $\sigma$ has essentially the same qualitative behavior versus rain rate; however, the error magnitude increases with increasing $\sigma$. The error in the rain rate derived from the near-surface reflectivity (after correction using the SRT-derived PIA) depends on both the near-surface reflectivity error and the PIA error. For the case shown in Fig. 1, the corrected reflectivity and the rain rate would be overestimated at very low rain rates and underestimated at moderate and high rain rates due to the domination of the PIA error. Although Nakamura (1991) did not analyze the near-surface reflectivity error for the half-filled, or binary, model, it is straightforward to show that in that case

$$Z_a^m/Z_u^m = 2^{b-1}10^{-0.2La[R^\beta-(R/2)^\beta]}. \tag{16}$$

At very low rain rates, the second factor, due to attenuation, is unity, and the factor $2^{b-1}$ is greater than unity (i.e., overestimation) for $b > 1$. This shows that when attenuation can be neglected, the nonlinearity of the $Z$–$R$ algorithm causes overestimation. However, as $R$ increases, the attenuation term becomes much less than unity, causing underestimation. At $R = 70$ mm h$^{-1}$ the near-surface reflectivity would be underestimated by 17 dB. This simple situation does not predict overestimation of reflectivity at high rain rates, as was found for the lognormal case.

The behavior of the near-surface reflectivity error is thus rather complicated as compared with the errors in the rain-top reflectivity and PIA. Even when the nonlinearity of the $Z$–$R$ relation is not included (i.e., $b$ is set to unity), at high rain rates there is severe overestimation for the lognormal case and severe underestimation for the binary case. Also, it must be remembered that we are considering the measured reflectivity, before any correction for attenuation, so the NUBF effects on the PIA are not relevant. The differences noted here can be understood by considering the nature of the two distributions. For the lognormal case, even though the mean rain rate is large, there will be some areas with light rain at the surface and, hence, light attenuation (due to the assumption of perfect vertical correlation). The return from these light rain areas may actually be greater than return from heavy rain areas due to severe attenuation in the heavy rain areas. These light rain areas can make the apparent reflectivity greater than the uniform reflectivity, corresponding to the mean, high rain rate. In the binary distribution, we only have areas with a high rain rate and severe attenuation and areas with no rain and, hence, no backscatter at all. There are no light rain, low attenuation areas. In this case, the uniform reflectivity is computed using the attenuation due to one-half the maximum rain rate. In contrast, when computing

the apparent reflectivity, all backscatter is attenuated using the maximum rain rate, making it smaller than the uniform reflectivity. However, if the binary model is extended to two nonzero rain rates, for example, $R_1$ and $R_2$, rather than $R$ and 0, both underestimation and overestimation can occur, depending on the magnitudes of $R_1$ and $R_2$. Thus, the sign of the error in the measured near-surface reflectivity is dependent on both the mean rain rate and the distribution of this rain within the footprint.

## 4. Data analysis technique

To quantify the effects of NUBF on real radar data, both spaceborne radar data and corresponding high-resolution data are needed. Currently, such data are not directly available, so we take the approach of simulating the spaceborne data using aircraft radar data, as was done by Amayenc et al. (1996). We simulate TRMM PR observations over ARMAR data in two steps. First, the ARMAR data is resampled to a uniform Cartesian grid; this is necessary because of aircraft motion, which causes the raw data to have nonuniform sampling. The resampling is performed by dividing the atmosphere in 60-m-thick horizontal slices. The locations of the closest ARMAR measurements, along with the corresponding reflectivity, are found for each slice. We then use linear interpolation to create a set of uniformly sampled reflectivities over each slice. The combination of all the horizontal slices gives a reflectivity volume with 60-m vertical spacing and 200-m horizontal spacing. The second step of the simulation involves convolving a multidimensional Gaussian function with the resampled data. The Gaussian is chosen so that it approximates both the range resolution (due to matched filtering in the receiver) and the two-way antenna pattern. One version of the simulation software uses a 3D Gaussian to simulate the TRMM PR resolution volume in the range direction and both the along-track and cross-track dimensions. The other version uses a 2D Gaussian to simulate the PR range and along-track resolution; the cross-track resolution is still that of ARMAR. Our approach neglects the finite resolution of the original ARMAR data. In a strict sense, the original data should first be deconvolved to remove the effects of the ARMAR antenna beam and range resolution. However, as noted by Amayenc et al. (1996), deconvolution is not practical. Furthermore, because of ARMAR's substantially better resolution, it is not necessary; the contribution of ARMAR's original finite resolution to the final resolution after convolution is quite small. The overall simulation approach taken here is similar to the 2D approach described in Amayenc et al. (1996) and the 3D approach described in Testud et al. (1996).

As discussed in Testud et al. (1996), a general simulation method must compute the attenuation to each range bin in the simulated spaceborne radar data. However, in our case, ARMAR and the TRMM PR have the same geometry and frequency. Hence, the attenuation experienced by a simulated PR bin is approximately the same as the attenuation already experienced by the ARMAR measurement. Consequently, we do not explicitly include attenuation in the simulation procedure. The convolution is thus implemented directly on ARMAR reflectivity to produce the PR reflectivity. The TRMM measured reflectivity $Z_a^m$ is given by

$$Z_a^m = \frac{\int Z^m(\bar{r})W(\bar{r})\delta(\bar{r})\, d\bar{r}}{\int W(\bar{r})\delta(\bar{r})\, d\bar{r}}, \tag{17}$$

where $Z^m$ is the measured (high resolution) ARMAR reflectivity, $W(\bar{r})$ is the Gaussian resolution function, $\bar{r}$ is the position vector, and the integrals are computed over the space corresponding to the PR resolution volume. As in the previous section, the subscript $a$ denotes apparent since (17) describes actual radar measurements rather than the reflectivity corresponding to an average rain rate. The function $\delta$ is an indicator function that takes on the value zero when ARMAR data is missing or invalid and unity when the ARMAR data is valid. After performing the convolution, thermal noise and fading noise appropriate to the TRMM PR can be added. Figure 2 shows an example of an along-track reflectivity profile acquired by ARMAR and by the simulated TRMM PR, using the 2D version of the simulation with thermal and fading noise included.

For the analysis of NUBF effects, we consider only data at nadir, and we do not add thermal or fading noise so that the results depend only on NUBF effects. Furthermore, only the 2D simulation approach is used. The reason for this is twofold. First, although ARMAR does scan across track, the swath width in the upper part of the storm may be less than the PR footprint. In the 3D simulation one must make assumptions about the missing reflectivity data in order to perform the averaging across track. Such assumptions are not needed in the 2D simulation since there is no cross-track averaging. Second, in the 3D simulation, the ARMAR across-track data used for a single TRMM PR footprint was acquired over approximately a 10° variation in the ARMAR antenna scan angle. For backscatter from rain, this is probably not critical. However, the change in ocean surface backscatter over a 10° change in incidence angle can be 10 dB. The ocean backscatter must therefore be corrected for incidence angle using a backscatter model and an assumed surface wind speed. For the 2D simulation, all averaging uses ARMAR data acquired at the same scan angle, so no assumptions about surface wind speed and backscatter models are needed.

The errors due to NUBF effects are found by comparing the uniform and apparent radar observables and rain rates. The apparent quantities are derived using the simulation technique discussed above. The uniform

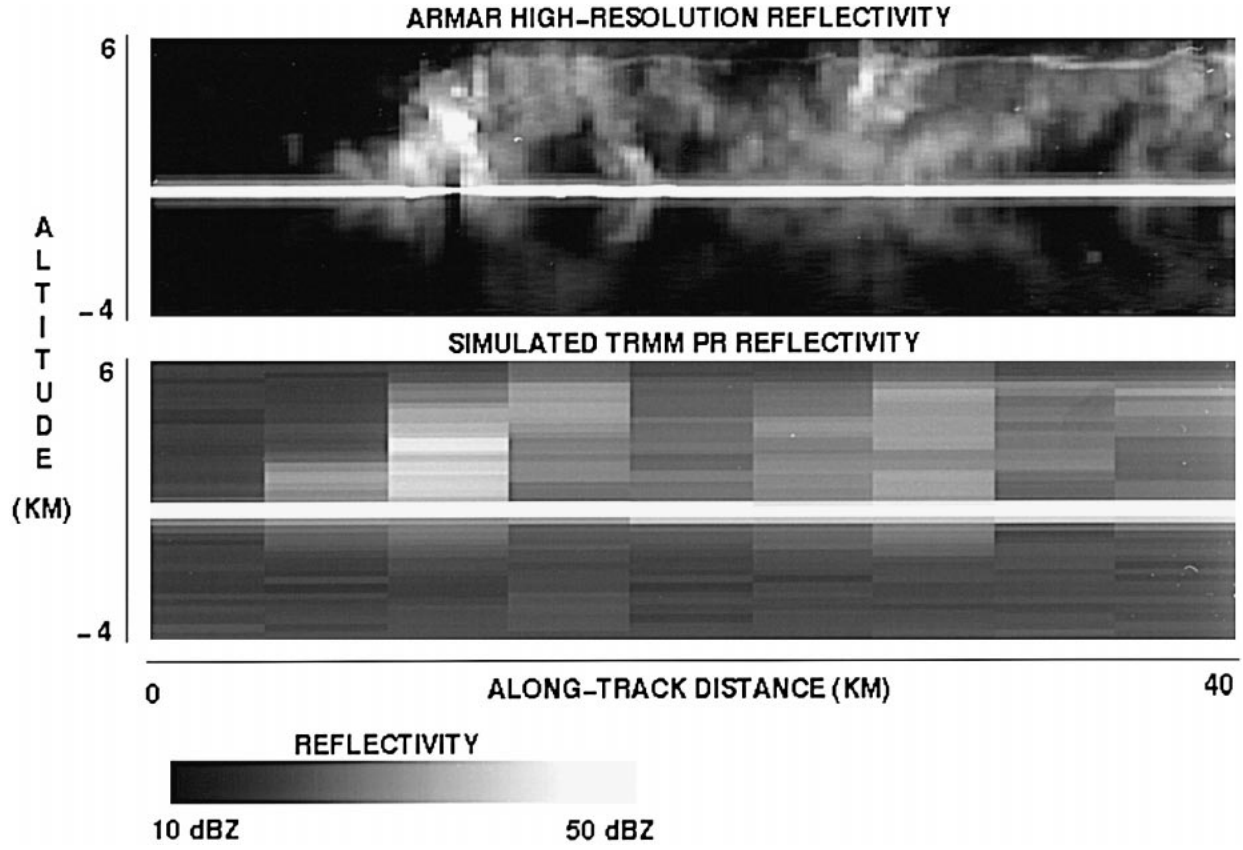


FIG. 2. ARMAR data from TOGA COARE, acquired at approximately 0230 UTC 18 January 1993. Vertical axis is altitude, and horizontal axis is along-track distance. Reflectivity ranges from 10 (black) to 50 dBZ (white). White horizontal line is return from ocean surface. Upper image is original high-resolution data; lower image is result of TRMM PR 2D simulation.

quantities correspond to the horizontally averaged rain rate and thus require the high-resolution rain rate. In section 3 this quantity was given; here, it is derived from the ARMAR reflectivity data with full horizontal resolution, but vertical resolution was degraded by convolution with the PR range weighting function. The differences between uniform and apparent quantities are thus due solely to horizontal variability of the rain rate. The uniform, or horizontally averaged, rain rate is defined by

$$R_u = \langle R \rangle = \frac{\int R(x)W'(x)\delta(x)\,dx}{\int W'(x)\delta(x)\,dx}, \qquad (18)$$

where $R(x)$ is the high-resolution rain rate, $W'$ is the weighting function that describes the area over which the averaging is computed, and $x$ is the along-track position in the radar footprint. The proper form for $W'$ can be found by noting the following corresponding equation for the TRMM PR apparent reflectivity:

$$Z_a^m = \frac{\int Z^m(x)W(x)\delta(x)\,dx}{\int W(x)\delta(x)\,dx}, \qquad (19)$$

which is derived from (17) by performing the integration over range. Now $Z^m(x)$ is the measured ARMAR reflectivity after range averaging, and $W(x)$ is the PR along-track antenna pattern. When attenuation is small, application of a linear $Z$–$R$ relation ($Z = aR$) to (19) yields an equation for the apparent rain rate that is identical in form to (18), except for $W(x)$, instead of $W'(x)$. In such a linearized case, the two rain rates must be equal, requiring that the weighting function $W'(x)$ used in (18) be the same as the along-track antenna pattern $W(x)$ in (19). This choice is necessary to exclude biases that are due simply to averaging over different volumes and not to nonlinearities. Thus, in summary, the uniform, or horizontally averaged, rain rate is found by performing the range portion of the integral in (17) on the ARMAR data, retrieving the rain rate from the resulting reflectivity profile, and horizontally averaging

TABLE 2. Computed apparent and uniform quantities.

| | Apparent | Uniform |
|---|---|---|
| PIA | $A_a$: found by applying SRT to simulated PR surface reflectivity | $A_u$: found from $2L\alpha\langle R_p\rangle^{\beta}$; i.e., Eq. (7) |
| PARR | $(-10 \log A_a/2L\alpha)^{1/\beta}$ | $\langle R_p\rangle = \langle(-10 \log A/2L\alpha)^{1/\beta}\rangle$; $A$ is high-resolution PIA from SRT |
| $Z^m$ (4 km) | $Z_a^m$ from PR simulation | $a\langle R\rangle^b$; i.e., Eq. (9) |
| Rain rate (4 km) | $(Z_a^m/a)^{1/b}$ | $\langle R\rangle = \langle(Z^m/a)^{1/b}\rangle$; $Z^m$ is measured high-resolution reflectivity |
| $Z^m$ (0.5 km) | $Z_a^m$ from PR simulation | $a\langle R\rangle^b A_u$; i.e., Eq. (11) |
| Rain rate (0.5 km) | $(Z_a^m/aA_a)^{1/b}$ | $\langle R\rangle = \langle(Z^m/aA)^{1/b}\rangle$ |

using (18) with $W'$ chosen as the along-track antenna pattern. Calculation of uniform radar observables is then based on the assumption that the uniform rain rate is spread uniformly over the antenna beam.

As discussed in section 3, there is a variety of algorithms for retrieving the rain rate. Here, we prefer to keep the results as general as possible and thus examine quantities that can provide insight into the effects of NUBF on several existing algorithms. As in section 3 we focus on the two-way PIA and the PARR, the near-surface (0.5-km altitude) reflectivity and rain rate, and the rain-top (4-km altitude) reflectivity and rain rate. The PIA is derived from the SRT. PARR is derived from the PIA, as discussed in the approximation leading to (6). The rain depth $L$ is 4.5 km, and the $k$–$R$ relation is given by (12). The rain-top rain rate is derived from the measured reflectivity using the $Z$–$R$ relation in (13); attenuation is neglected. The near-surface rain rate is derived by first increasing the measured reflectivity by the SRT-derived PIA. The resulting attenuation-corrected reflectivity is then converted to rain rate using (13). At the rain top, the Hitschfeld–Bordan solution (without path attenuation constraint) and the $\alpha$-adjustment algorithm (Meneghini et al. 1983) should give the same results as the $Z$–$R$ method used here. Likewise, our method of retrieving surface rain rate should be identical to both the $\alpha$-adjustment algorithm and the $kZS$ algorithm (Marzoug and Amayenc 1994). Our results for the near-surface rain are not applicable to the unconstrained Hitschfeld–Bordan technique; however, this technique is only applicable to light rain (Iguchi and Meneghini 1994). Finally, our results on the PIA should apply to all algorithms that use the SRT-derived PIA (e.g., Meneghini et al. 1983; Marzoug and Amayenc 1994). Table 2 summarizes the quantities to be compared. The PIA and reflectivities in Table 2 are analogous to the quantities defined in (6)–(11) for the theoretical analysis in section 3.

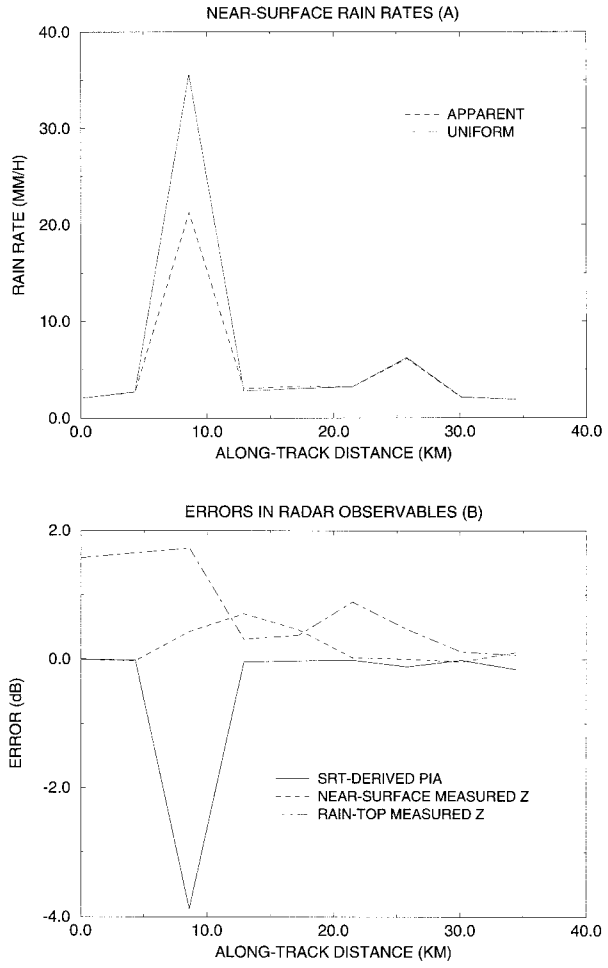


FIG. 3. Plots of quantities computed for the case in Fig. 2: (a) uniform rain rate (solid) and apparent rain rate (dashed). (b) Errors in two-way PIA (solid), rain-top measured reflectivity (dotted–dashed), and near-surface measured reflectivity (dashed).

## 5. Results

We begin by considering the NUBF effects for the case displayed in Fig. 2. This case consists of a rather

TABLE 3. Statistics of NUBF errors (apparent minus uniform).

| Parameter | Mean | Std dev | Min | Max |
|---|---|---|---|---|
| PIA (dB) | −0.2 | 0.8 | −11.7 | 0.0 |
| PARR (mm h$^{-1}$) | −0.5 | 1.7 | −22.6 | 0.0 |
| Rain-top $Z$ (dB) | 0.3 | 0.5 | 0.0 | 4.7 |
| Rain-top $R$ (mm h$^{-1}$) | 0.1 | 0.1 | 0.0 | 2.3 |
| Near-surface $Z$ (dB) | 0.0 | 0.8 | −12.3 | 10.5 |
| Near-surface $R$ (mm h$^{-1}$) | −1.0 | 5.5 | −78.7 | 18.1 |

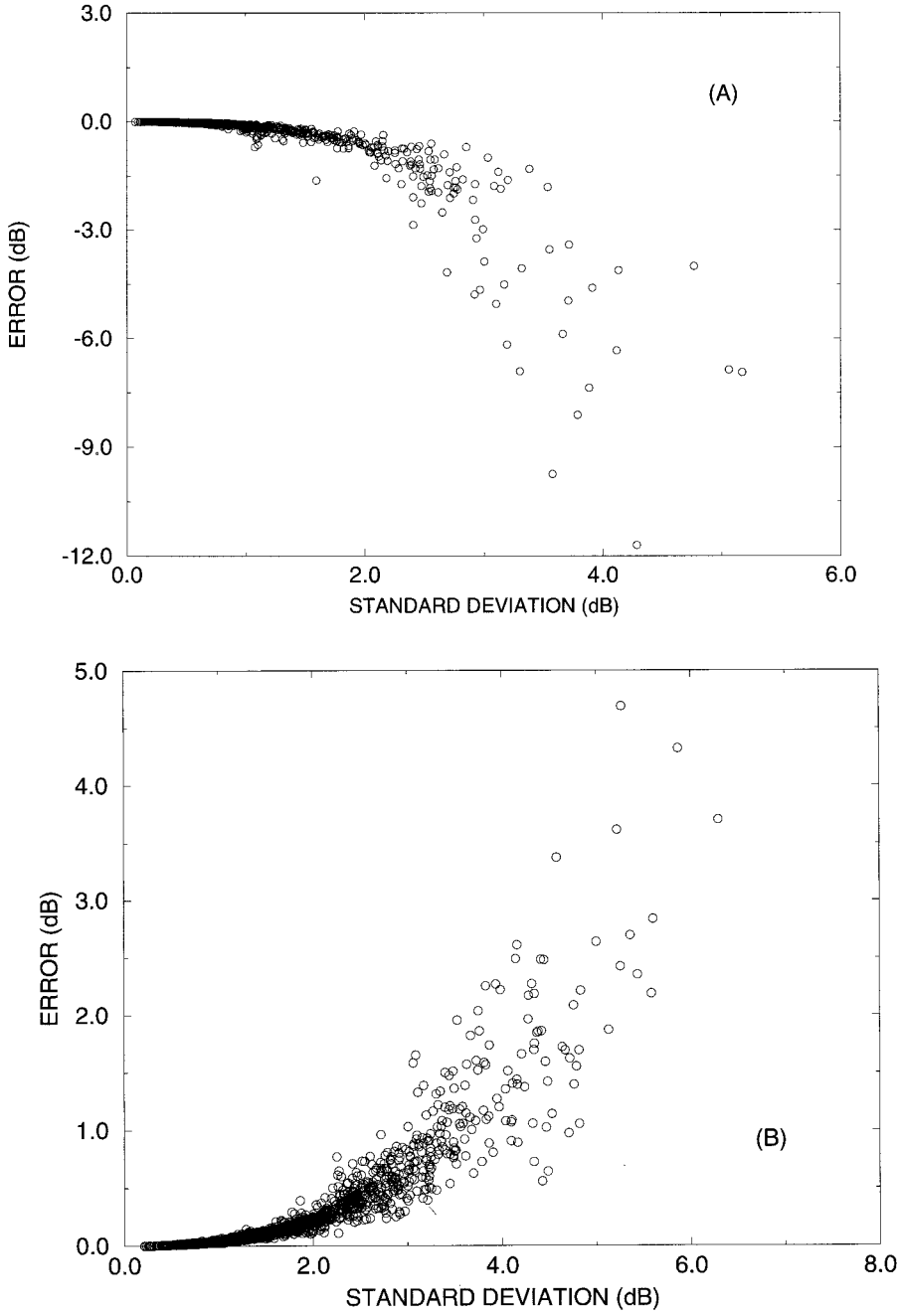


FIG. 4. (a) Scatterplot of the two-way PIA error vs the standard deviation of the high-resolution two-way PIA within the footprint. (b) Scatterplot of the error in reflectivity at 4-km altitude vs standard deviation of high-resolution reflectivity at 4 km within the footprint. (c) Scatterplot of the error in the near-surface reflectivity vs standard deviation of high-resolution near-surface measured reflectivity within the footprint.

strong convective cell at left, with lighter mixed convective and stratiform rain to the right. Figure 3a compares the uniform and apparent surface rain rates. The apparent near-surface rain rate is similar to the uniform rain rate, except in the intense convective cell, where it is significantly smaller. There, the uniform is 36 mm $h^{-1}$, while the apparent rain rate is 21 mm $h^{-1}$. Figure 3b shows the error (apparent minus uniform in terms of decibels) in the PIA, near-surface reflectivity, and 4-km reflectivity. The largest error is in the PIA, which is underestimated by 3.9 dB in the convective cell. At the location of the maximum PIA error, the measured re-

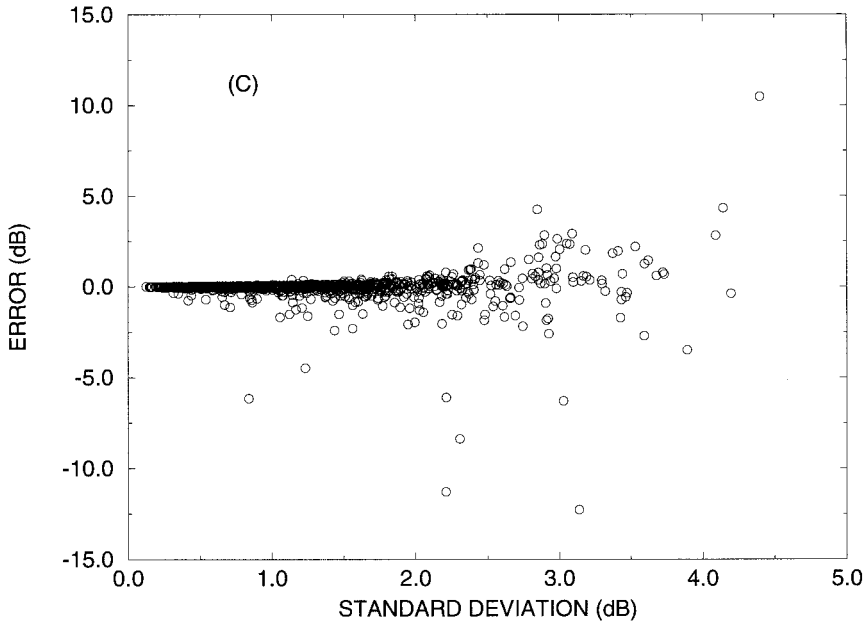


FIG. 4. (*Continued*).

flectivity near the surface is slightly overestimated (0.4 dB); however, when corrected by the erroneous PIA, the surface reflectivity is underestimated by 3.5 dB. When this is converted to rain rate using the *Z–R* relation, the rain rate is thus underestimated. At 4-km altitude the reflectivity is overestimated by a maximum of 1.7 dB.

Table 3 shows the statistics of NUBF errors (apparent minus uniform) over all of TOGA COARE. These statistics are based on the 1397 simulated PR footprints with a uniform, or horizontally averaged, PARR of more than approximately 2 mm $h^{-1}$. While the means and standard deviations of the errors in all quantities are relatively small, the distributions have long tails; that is, there are some cases with very large errors, as can be seen by the minimum and maximum errors. Also, for some quantities, the errors are only positive or only negative. The apparent PIA and PARR are always underestimated relative to the uniform quantities (i.e., negative errors). The greatest underestimation is approximately 12 dB for the PIA and 23 mm $h^{-1}$ for the PARR. The maximum uniform PARR for the cases summarized in Table 3 was 71 mm $h^{-1}$, with a mean of 12 mm $h^{-1}$. The PARR normalized standard deviation $\sigma$, defined in section 3, has a mean of 0.25 and a maximum of 3.4. The model calculations in section 3 were performed for similar values of PARR and $\sigma$ and predict similar values of underestimation of the PIA (Fig. 1). Previous studies using simulated data and smaller sets of real radar data have also noted underestimation of the PIA (e.g., Nakamura 1991; Amayenc et al. 1993; Kozu and Iguchi 1996). If we compute the average PARR over all 1397 footprints, we find that the average using the apparent PARR is underestimated by 4%.

The reflectivity and rain rate at 4-km altitude are always overestimated, as was the case in the model calculations in section 3. For the cases summarized in Table 3, the observed mean rain rate at 4-km altitude ranges from near zero to 16 mm $h^{-1}$ with a mean of 2.4 mm $h^{-1}$. The normalized standard deviation $\sigma$ for the 4-km rain rate has a mean of 0.65 and a maximum of 2.2. The mean $\sigma$ for this case is higher than observed for the PARR. This may be related to the decorrelation of the rain rate in the vertical dimension, which causes the variations in rain rate at each altitude to add incoherently, reducing the path-averaged rain rate (and PIA) variability. Since attenuation is neglected in retrieving the rain at 4 km, these results are characteristic of rain retrieval using a *Z–R* relation. Previous authors have also noted overestimation due to the nonlinearity of the *Z–R* relation (e.g., Nakamura 1991; Amayenc et al. 1996). When comparing the TOGA COARE average rain rates using both the high-resolution rainfall and the rainfall from the simulated TRMM PR, we find an overestimation by 3%, which is similar to the findings of Amayenc et al. (1996) for the *Z–R* algorithm. The maximum overestimation of reflectivity is 4.7 dB; however, this error occurred at a low uniform reflectivity (18 dB*Z*), and the absolute rain-rate error made in this case was only 0.3 mm $h^{-1}$. At higher reflectivities ($>$35 dB*Z*) the maximum reflectivity error is around 1 dB, resulting in a rain-rate error of 1.4 mm $h^{-1}$. The maximum rain-rate overestimation is 2.3 mm $h^{-1}$, occurring for a case with 34 dB*Z* uniform reflectivity.

The errors in the measured near-surface reflectivity are both negative and positive, extending from $-12.3$ to $+10.5$ dB. The mean error is very close to zero, and the error distribution is fairly symmetric. The observed mean near-surface rain rate for these cases ranges from

0.7 to 390 mm $h^{-1}$ with a mean of 8.8 mm $h^{-1}$. The normalized standard deviation $\sigma$ for the near-surface rain rate has a mean of 0.44 and a maximum of 1.5. These observations of both negative and positive errors are qualitatively consistent with the model calculations in section 3. There it was also found that the error could be positive or negative, depending on both the mean rain rate and the distribution of rain within the PR footprint.

While the near-surface reflectivity error is equally likely to be positive or negative, the near-surface rain rate error is negative more often than positive, and the maximum negative error is approximately $-79$ mm $h^{-1}$. In contrast, the maximum positive error is only 18 mm $h^{-1}$. The average rain rate at the surface, computed over all 1397 footprints, is underestimated by 11%, similar to the findings of Amayenc et al. (1996) for the *kZS* algorithm at 35 GHz. Near-surface rainfall underestimation has also been noted in other studies (e.g., Testud et al. 1996). The reason that the near-surface rain rate is typically underestimated even though the near-surface reflectivity error has zero mean is that the rain rate is derived by correcting the apparent measured reflectivity by the apparent PIA, which is always underestimated. The resulting rain rate is overestimated only in those cases in which the reflectivity overestimation error is larger than the PIA underestimation error.

Figure 4 shows scatterplots of the measurement errors versus the standard deviation of the high-resolution measurements within the footprint. The standard deviation is derived using the measured reflectivity in the linear domain and is then converted to decibels. In Fig. 4a the error in PIA is correlated with the standard deviation of the PIA within the PR footprint (linear correlation coefficient $r = -0.77$), although the scatter is rather large. Largest PIA errors occur when the PIA standard deviation is large. It should be noted that the PIA standard deviation could have also been computed in the log domain rather than the linear domain. The PIA standard deviation based on computation in the log domain is roughly a factor of 2 larger than the PIA standard deviation shown in Fig. 4a. In Fig. 4b the error in the 4-km altitude reflectivity is correlated with the standard deviation of the high-resolution 4-km altitude reflectivity ($r = 0.86$). As is the case in Fig. 4a, the scatter is large. Figure 4c shows the near-surface reflectivity error versus the standard deviation of the near-surface reflectivity. It can be seen that the magnitude of the error typically increases with increasing standard deviation. However, the error sign can be positive or negative, so that the mean error is still close to zero even for large standard deviations. It should also be noted that the large standard deviations generally correspond to convective rain with high rain rates. If we consider the near-surface reflectivity errors for cases with a near-surface uniform rain rate of greater than 50 mm $h^{-1}$, the mean near-surface reflectivity error is still very close to zero. This result suggests a deviation from lognormal statistics since the model calculations in Fig. 1 for high rain rates and lognormal statistics predict large positive errors. Kozu and Iguchi (1996) also found that the rain rate within the PR footprint may not always be lognormal.

While the NUBF errors found in this study are usually small, they can have nonzero mean, causing biases in rain-rate estimates. Therefore, it is desirable to correct for NUBF effects so that the rain-rate estimates are not biased. However, as pointed out by Testud et al. (1996), correction of NUBF errors is a difficult problem because of their dependence on numerous factors. This was illustrated by Fig. 4, in which there can be a large variation in the error even for a given within-footprint variability. Nevertheless, a correction procedure for the PIA is discussed in Kozu and Iguchi (1996) and is shown to reduce NUBF errors when applied to ship-based radar data.

Ideally, a correction procedure would correct both the PIA and the complete reflectivity profile. However, the largest biases found in this study were due to the PIA error, so its correction would appear to be first priority. Figure 4a showed that although there is considerable scatter, the PIA error is, indeed, correlated with the high-resolution PIA standard deviation, denoted by $s_0$. Using a least squares fit to the data in Fig. 4a, the uniform PIA can be estimated from the apparent PIA and $s_0$ using

$$A_u = A_a + 0.1 - 0.45s_0 + 0.42s_0^2, \qquad (20)$$

where $A_u$, $A_a$, and $s_0$ are expressed in decibels. Application of this equation to correct the apparent PIA reduces the bias in PARR over TOGA COARE from $-4\%$ to 0% and the bias in near-surface rain rate from $-11\%$ to $+2\%$. The correction procedure suggested here is not expected to be directly applicable to PR data because it was derived using 2D averaging. However, a similar correction derived using nonattenuating, surface-based radar data in three dimensions could yield a correction procedure directly applicable to the TRMM PR.

An alternative is to derive a correction procedure using the model in section 3. It is straightforward to compute the uniform PIA versus the apparent PIA for different values of $\sigma$ (similar to the curves showing PIA error versus rain rate for different $\sigma$ in Fig. 1). Each $A_u$ versus $A_a$ curve (with both quantities expressed in decibels) can be well approximated as a power law whose coefficients depend on the value of $\sigma$. Thus, given $\sigma$ and $A_a$, an estimate of $A_u$ can be found and used in rain retrieval. In applying this approach, we find a reduction in biases similar to those noted above for the empirically based technique using (20). This model-based approach is similar to that used by Kozu and Iguchi (1996).

Both the empirically based correction (20) and the model-based correction require the high-resolution standard deviation of the PIA, which cannot be directly observed by a spaceborne radar. Kozu and Iguchi (1996) found reasonably good correlation between the low- and high-resolution standard deviations using data from

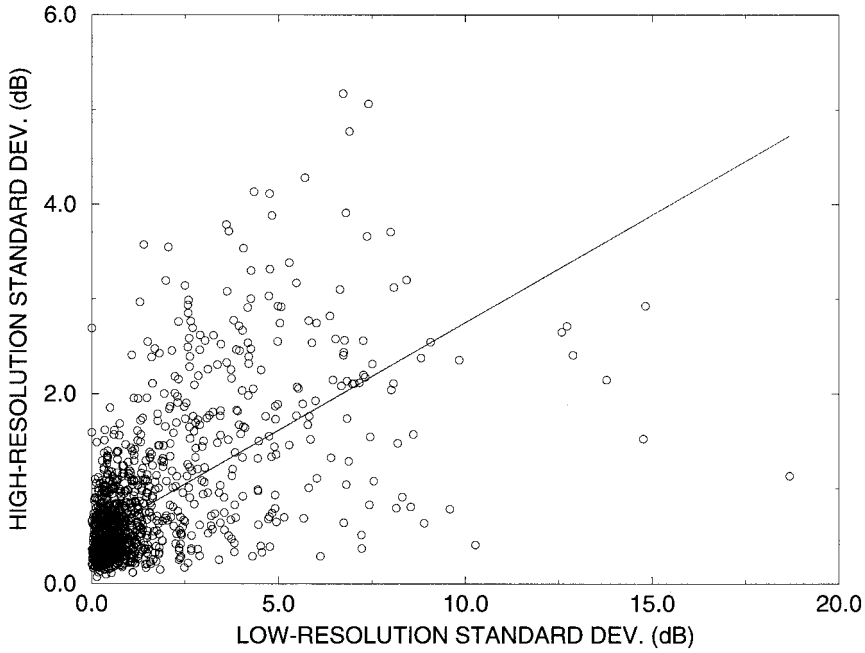


FIG. 5. Scatterplot of the high-resolution PIA standard deviation vs the low-resolution PIA standard deviation estimated from three along-track PR footprints. Also shown is the linear regression line (correlation coefficient $r = 0.62$).

ship-based radar. The low-resolution standard deviation was estimated from a $3 \times 3$ box of simulated TRMM PR footprints. Kummerow and Giglio (1994) also found correlation between low- and high-resolution measures of variability using data from ground-based radar. Because we have limited our study to 2D data, we compute the low-resolution standard deviation (in the log domain) based on three along-track footprints rather than a $3 \times 3$ box. Figure 5 shows a scatterplot of the high-resolution PIA standard deviation $s_0$ versus the low-resolution PIA standard deviation $s_1$. Using linear regression, we find that

$$s_0 = 0.48 + 0.23s_1, \tag{21}$$

where $s_0$ and $s_1$ are both in decibels. Although the scatter is quite large, due at least in part to the use of only three samples in computing $s_1$, the two quantities are correlated ($r = 0.62$).

## 6. Conclusions

We have presented the results of a study of errors due to nonuniform beam filling in a simulated radar with along-track resolution equal to that of the TRMM PR. Our study has focused on path-integrated measurements, as derived using the surface reference technique, rain-top measurements using the *Z–R* relation without attenuation correction, and near-surface measurements using the surface reference technique for attenuation correction and the *Z–R* relation. We first presented results of theoretical calculations showing underestimation of the PIA and overestimation of the rain-top reflectivity. The model also showed that the near-surface reflectivity could be underestimated or overestimated, depending on the rain-rate mean and distribution. We then presented observational results using a large set of TOGA COARE airborne radar data, collected with the TRMM PR frequency and scanning geometry. We examined the errors in rain-rate estimation and found results similar to those from previous studies: underestimation of the path-averaged rain rate (always), underestimation of the near-surface rain rate (typically), and overestimation of the rain-top rain rate (always). We also compared the PIA and reflectivity profile measured by the PR with those corresponding to the horizontally averaged rain rate. We found that relative to the desired values, the PIA is always underestimated, the rain-top reflectivity is always overestimated, and the near-surface reflectivity is underestimated roughly as often as it is overestimated. The largest errors occur for the near-surface rain rate; over TOGA COARE the average is underestimated by 11%. We found that the bias in the estimated near-surface rain rate is caused primarily by the PIA error. Correction techniques for the PIA using the high-resolution PIA standard deviation reduced the bias. While the high-resolution PIA standard deviation is not directly measurable by a spaceborne radar, it is correlated with the low-resolution standard deviation, which can be measured by a spaceborne radar.

*Acknowledgments.* The authors would like to thank the anonymous reviewers for their comments and sug-

gestions, which helped to improve the clarity and accuracy of this paper. The research described here was performed by the Jet Propulsion Laboratory, California Institute of Technology, under contract with the National Aeronautics and Space Administration (NASA). Support from the NASA TRMM Science Program is gratefully acknowledged.

## REFERENCES

Amayenc, P., M. Marzoug, and J. Testud, 1993: Analysis of cross-beam resolution effects in rainfall rate profile retrieval from a spaceborne radar. *IEEE Trans. Geosci. Remote Sens.,* **31,** 417–425.

——, J. P. Diguet, M. Marzoug, and T. Tani, 1996: A class of single- and dual-frequency algorithms for rain-rate profiling from a spaceborne radar. Part II: Tests from airborne radar measurements. *J. Atmos. Oceanic Technol.,* **13,** 142–164.

Durden, S. L., E. Im, F. K. Li, W. Ricketts, A. Tanner, and W. Wilson, 1994: ARMAR: An airborne rain mapping radar. *J. Atmos. Oceanic Technol.,* **11,** 727–737.

Goldhirsh, J., and B. Musiani, 1986: Rain cell size statistics derived from radar observations at Wallops Island, Virginia. *IEEE Trans. Geosci. Remote Sens.,* **GE-24,** 947–954.

Graves, C. E., 1993: A model for the beam-filling effect associated with the microwave retrieval of rain. *J. Atmos. Oceanic Technol.,* **10,** 5–14.

Ha, E., and G. R. North, 1995: Model studies of the beam-filling error for rain-rate retrieval with microwave radiometers. *J. Atmos. Oceanic Technol.,* **12,** 268–281.

Hitschfeld, W., and J. Bordan, 1954: Errors inherent in the radar measurement of rainfall at attenuating wavelengths. *J. Meteor.,* **11,** 58–67.

Houze, R. A., 1981: Structures of atmospheric precipitation systems: A global survey. *Radio Sci.,* **16,** 671–689.

Iguchi, T., and R. Meneghini, 1994: Intercomparison of single-frequency methods for retrieving a vertical rain profile from airborne or spaceborne radar data. *J. Atmos. Oceanic Technol.,* **11,** 1507–1516.

Kedem, B., L. S. Chiu, and G. R. North, 1990: Estimation of mean rain rate: Application to satellite observations. *J. Geophys. Res.,* **95,** 1965–1972.

Kozu, T., and T. Iguchi, 1996: A preliminary study of non-uniform beam filling correction for spaceborne radar rainfall measurement. *I.E.I.C.E. Trans. Comm.,* **E79-B,** 763–769.

Kummerow, C., and L. Giglio, 1994: A passive microwave technique for estimating rainfall and vertical structure information from space. Part I: Algorithm description. *J. Appl. Meteor.,* **33,** 3–18.

Lopez, R. E., 1977: The lognormal distribution and cumulus cloud populations. *Mon. Wea. Rev.,* **105,** 865–872.

Marzoug, M., and P. Amayenc, 1994: A class of single- and dual-frequency algorithms for rain-rate profiling from a spaceborne radar. Part I: Principle and tests from numerical simulations. *J. Atmos. Oceanic Technol.,* **11,** 1480–1506.

Meneghini, R., 1978: Rain-rate estimates for an attenuating radar. *Radio Sci.,* **13,** 459–470.

——, J. Eckerman, and D. Atlas, 1983: Determination of rain rate from a spaceborne radar using measurements of total attenuation. *IEEE Trans. Geosci. Remote Sens.,* **GE-21,** 34–43.

Nakamura, K., 1991: Biases of rain retrieval algorithms for spaceborne radar caused by nonuniformity of rain. *J. Atmos. Oceanic Technol.,* **8,** 363–373.

——, K. Okamoto, T. Ihara, J. Awaka, T. Kozu, and T. Manabe, 1990: Conceptual design of rain radar for the Tropical Rainfall Measuring Mission. *Int. J. Satellite Comm.,* **8,** 257–268.

Olsen, R. L., D. V. Rogers, and D. B. Hodge, 1978: The $aR^b$ relation in the calculation of rain attenuation. *IEEE Trans. Antennas Propagat.,* **AP-26,** 318–329.

Schroeder, L. C., P. R. Schaffner, J. L. Mitchell, and W. L. Jones, 1985: AAFE RAD-SCAT 13.9 GHz measurements and analysis: Wind-speed signature of the ocean. *IEEE J. Oceanic Eng.,* **OE-10,** 346–357.

Simpson, J., R. F. Adler, and G. R. North, 1988: A proposed Tropical Rainfall Measuring Mission (TRMM) satellite. *Bull. Amer. Meteor. Soc.,* **69,** 278–295.

Testud, J., P. Amayenc, X. K. Dou, and T. F. Tani, 1996: Tests of rain profiling algorithms for a spaceborne radar using raincell models and real data precipitation fields. *J. Atmos. Oceanic Technol.,* **13,** 426–453.

Webster, P. J., and R. Lukas, 1992: TOGA COARE—The Coupled Ocean–Atmosphere Response Experiment. *Bull. Amer. Meteor. Soc.,* **73,** 1377–1416.